JES Focus Issue on Ubiquitous Sensors and Systems for IoT

Integrated Flexible Conversion Circuit between a Flexible Photovoltaic and Supercapacitors for Powering Wearable Sensors

J. O. Thostenson,[1] Z. Li,[1] C. H. J. Kim,[2] A. Ajnsztajn,[3] C. B. Parker,[1,z] J. Liu,[2] A. V. Peterchev,[1,4,5,6] J. T. Glass,[1,*] and S. M. Goetz[1,4,6]

[1]*Department of Electrical and Computer Engineering, Duke University, Durham, North Carolina 27708, USA*
[2]*Department of Chemistry, Duke University, Durham, North Carolina 27708, USA*
[3]*Department of Mechanical Engineering and Material Science, Duke University, Durham, North Carolina 27708, USA*
[4]*Department of Psychiatry and Behavioral Sciences, Duke University, Durham, North Carolina 27710, USA*
[5]*Department of Biomedical Engineering, Duke University, Durham, North Carolina 27708, USA*
[6]*Department of Neurosurgery, Duke University, Durham, North Carolina 27710, USA*

Integration of an organic photovoltaic (PV) with carbon-based supercapacitors (SCs) into a system for solar energy harvesting and storage is interesting for off-grid applications such as mobile electronics and sensor systems. Presented here is a conversion and control circuit (CC) on a flexible polyimide substrate in an integrated flexible energy harvesting and storage device compatible with roll-to-roll manufacturing (R2R). The CC is capable of PV max power-point tracking, DC-DC voltage boost of the PV output across a bank of four SCs, and charge balancing across the bank of SCs. This system is compared to a conventional direct connection between the PV and the SCs. More energy can be harvested from the PV and stored in the SC bank when using the CC to drive the PV at peak power, boost the output voltage, and balance it across serial connection of SCs. Finally, the CC, PV, and SCs are mounted to a 3D printed substrate and circuit which is used to power a wearable sensor. Due to these benefits and ability to be integrated with R2R, the presented CC provides a practical means of improving wearable solar energy harvesting and storage systems.
 [DOI: 10.1149/2.0141808jes]

Manuscript submitted February 9, 2018; revised manuscript received March 23, 2018. Published April 25, 2018. *This paper is part of the JES Focus Issue on Ubiquitous Sensors and Systems for IoT.*

In the flexible electronics literature, multiple publications demonstrated novel energy materials and devices, such as thin-film flexible photovoltaics (PVs)[1–10] and carbon-based supercapacitors (SCs)[11–18] that are roll-to-roll (R2R) compatible. A few publications have further integrated a PV material with SCs to form an energy device capable of solar energy harvest and storage.[17,19–24] Although simply connecting the devices without a conversion and control circuit (CC) that controls the flow of charge and the load impedance experienced by the PV can harvest and store energy, there are three problems that arise from this configuration: (i) the PV elements are operated inefficiently at suboptimal voltage–current conditions, far from the maximum-power point (MPP), (ii) undercharging the SCs due to low PV output voltage, and (iii) unbalanced charge storage across a bank of SCs with the risk of overcharging some while undercharging other SCs as well as a low usable combined capacity. These problems result in an inefficient and impractical energy device. In large PV systems, a CC typically mitigates these problems. However, such CCs use a discrete design with stiff bus bars or rigid circuit boards, which are incompatible with the flexible film design of the rest of the system. The lack of availability of a R2R-compatible CC has limited the realization of a R2R energy fabric for practical applications such as wearable sensors and the internet of things (IoT).[25]

Many techniques have been developed to enable R2R-compatible packaging of CCs. Within the CC architecture, switching-mode DC-DC boost converters have been given considerable attention. For example, Z-folded flexible planar transformers have been developed that allow R2R production.[26] Planar geometries of flexible foils for use as low-profile inductors[27] and flip-chip flex-circuit packaging techniques have also been developed for intelligent power modules.[28] Additionally, several power converter prototypes constructed on flexible materials have been reported.[29,30] Due to higher power needs and surface area constraints, these devices are not suitable for low-wattage and fabric-based applications.

Flexible PVs are low-wattage components ($< 10\ \mathrm{mW \cdot cm^{-2}}$) with thin geometries. Whereas commercially available flexible PVs, such as Infinity PV, have areas on the order of 100 $\mathrm{cm^2}$ with power outputs under AM1.5G illumination on the order of 500 mW, most commercially available CCs are designed for > 10 W applications and are not flexible. In the case of wearable sensors, energy fabrics and increasing off-grid IoT devices, there is a need for a CC capable of efficient low-wattage operation that is flexible.[31–42]

In this work, we report a novel CC that is compatible with R2R manufacturing for integration with energy materials and wearable sensors. The CC incorporates a DC-DC buck-boost converter that accepts a PV input voltage range of 0.3–5.5 V and boosts to an adjustable output voltage range of 2–5.2 V across a bank of four SCs. The converter further tracks the PV MPP and adjusts its input impedance to maximize the power. The boosted voltage can be balanced across each SC at 1.25 V for use with dissimilar SCs and to have a margin of safety with 1.5 V devices. Finally, the flexibility and utility of the CC is demonstrated through integration with a flexible 3D-printed substrate and used to power a typical wearable sensor load. This work contributes to the realization of a wearable energy fabric that is capable of both solar energy harvesting and storage through the integration of a flexible and R2R compatible CC for use with powering ubiquitous sensors and systems for the IoT.

Methods

Construction of conversion and control circuit.—Figure 1 shows an overview schematic and a picture of the constructed conversion and control circuit (CC). The CC is connected with 1 photovoltaic (PV) module, up to 4 supercapacitors (SCs), and a sensor load. The PV and SCs interface with the CC using a non-isolated boost converter and an embedded MPP tracking (MPPT) algorithm. The boost converter incorporates an n-channel low-side ($r_{\mathrm{ds,on}} \approx 120\ \mathrm{m\Omega}$) and a synchronously rectifying p-channel high-side field-effect transistor ($r_{\mathrm{ds,on}} \approx 140\ \mathrm{m\Omega}$). Despite its lower power performance, such as higher resistance and higher gate charge, the p-channel transistor

*Electrochemical Society Member.
[z]E-mail: charles.parker@duke.edu

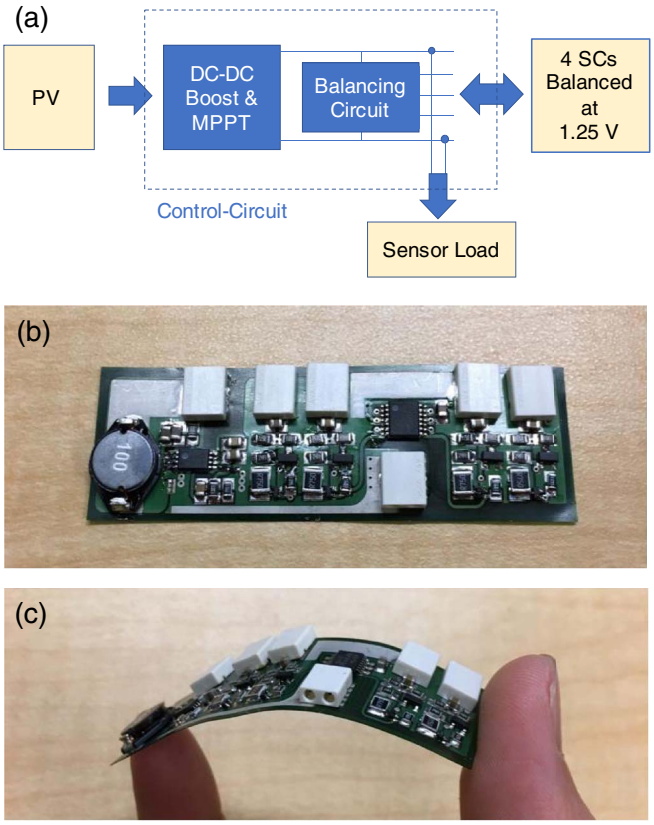

Figure 1. (a) Schematic of conversion and control circuit (CC) that manages the flow of charge between the PV, 4 SCs, and a sensor load, (b) picture of the constructed circuit, and (c) demonstration of its flexibility, showing compatibility with R2R manufacturing.

is overall advantageous for low-power energy harvesting as it can be controlled entirely with voltages below or at the input voltage and does not require a more complicated gate drive circuit.[43] The converter uses a surface-mount ferrite inductor with 10 µH and an internal resistance of 100 mΩ for boosting. The switching rate of the transistors is 100 kHz. The MPPT is based on the perturb-and-observe method[25] and operates at 100 Hz. Size and loss considerations were the basis for the moderate switching frequency. Whereas a higher switching frequency is indeed able to reduce the size of passives, particularly the inductor, switching loss grow. However, the size of our electronics is mostly dominated by the connectors. The boost conversion and MPPT moderate the voltage requirements of both solar harvesting and storage to enable efficient energy conversion and complete use of the storage capacity. On the SC side of the CC, a balancer is implemented that uses the dissipative shunting technique.[27] The CC was designed with two conducting layers, each with 18 µm thickness of copper on a 50 µm polyimide substrate (KCL 3–17/50 HT, Krempel GmbH), which was processed in a normal photo-lithographic etching process. The substrate and the adhesive between the copper and the substrate are rated for at least 150°C. The electronic components are all on the same side for a clean integration with the flexible PV and SCs, although this is not necessary.

Measurement of charging with and without conversion and control circuit.—Figure 2 shows an overview of the measurement apparatus used in section Comparison of charging with and without conversion and control circuit. For section Comparison of equal capacitance SC charging directly and with a CC, voltage measurements were made across the PV (Pionovasion CIGS Solar Cloth SN# 13071200082, 2.6 V and 2.5 W) and 4 SCs (Maxwell Tech. BCAP0005, 5 F and 2.5 V window) with a NI USB 6009 data acquisition unit (National Instruments). Measurement of the PV photocurrent was made through a serial connection on the positive lead using a Keysight 34461A digital multimeter. Both the voltage and current measurements were recorded using *LabView* run on a connected PC. The PV was illuminated with an AM1.5 G light source (Newport Oriel) at 1 sun and 0.75 sun intensities. Both intensities under-filled the PV. The voltage and current were continuously measured during charging of the SCs by the PV with and without the CC. Power and energy measurements were taken from the voltage and current with respect to time for the PV and the SCs.

In section One sun charging of SCs with non-equal capacitances, the same measurements were repeated–this time using 1 sun illumination intensity and 4 SCs that differed in capacitance. 1 F (2x, Maxwell Tech. BCAP0001, 2.7 V), 5 F (Maxwell Tech. BCAP0005, 2.7 V), and 10 F (Maxwell Tech. BCAP001, 2.7 V) supercapacitors were used.

Construction of sensor load and flexible substrate.—To demonstrate the flexibility and practical use of the CC, we constructed a sensor on a 3D printed flexible substrate. The sensor demonstration consisted of a microcontroller (Sparkfun DEV-12587, 3.3 V/8 MHz), two atmospheric sensors for pressure, temperature and humidity (Sparkfun SHT15 and MPL3115AA2) and a 16 × 2 pixel LCD display (Sparkfun

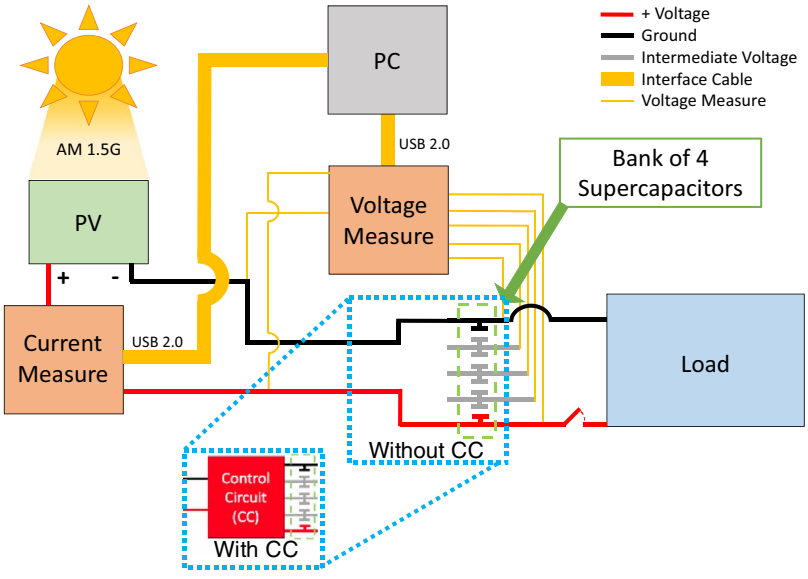

Figure 2. Measurement apparatus used for comparing charging of the SCs from the PV with and without the CC. Measurements of voltage are taken across the PV and each SC.

ADM2004U-FL-YBS). The sensor demonstration was programmed to refresh the LCD display every 5 seconds. Refreshing took less than 1 s. Power requirements of the demonstration were measured to be 23 μW during idle and 132 μW during refresh.

A flexible substrate for integrating the PV, SCs and CC components together was 3D printed with the fused deposition modeling (FDM) technique. The substrate was fabricated using black Hatchbox PLA dielectric material (UPC number 849344024248). The substrate was 0.8 mm thick, ensuring that the fabricated substrate would be sufficiently flexible. The conductive traces were printed using Electrifi, a highly conductive thermoplastic material (Multi3D SKU: electrifi100) developed by the Wiley Research Group at Duke University. The Electrifi material is a mechanically flexible compound with a volume resistivity of 0.006 $\Omega \cdot$ cm.[44] The dimensions of the conductive traces were 1 mm high × 2 mm wide. The PLA material was printed at 190°C at 30 mm $\cdot$ s^{-1} and the Electrifi material was printed at 140°C at 15 mm $\cdot$ s^{-1}. A 0.5 mm diameter nozzle was used for both materials and layer height was set at 0.2 mm. A heated bed was not used for printing to maintain the conductivity of the Electrifi material. BuildTak was used as the primary build platform, as it is compatible with PLA without a heated bed. The components were electrically connected using the printed conductive traces. When needed, conductive screws and wire were connected between the traces and components. Components were secured to the board using adhesive (Loctite Black Max 380) or screws.

Results and Discussion

Operational input-range and efficiency of conversion and control circuit.—Directly connecting a photovoltaic (PV) to supercapacitors in series without a conversion and control circuit (CC) may harvest and store solar energy, but it will not fully use the storage capacity of the SCs. In this case, the PV is not guaranteed to work at the MPP and the charge storage capacity of the SCs is underutilized due to miss-matching of PV and SC voltages and voltage imbalance among SCs caused by a manufacturing spread of the individual capacities. Thus, we designed and built the CC using a non-isolated boost converter and an embedded MPPT algorithm. The MPPT is based on the perturb-and-observe method[25] and operates at 100 Hz. The boost conversion and MPPT match and moderate the voltage requirements of both the harvesting and the storage sides. Furthermore, balancing of the SC voltages ensures equal charging levels and avoids overvoltage on individual SC, e.g., due to a smaller capacity associated with production tolerances and ageing. We implemented a top balancer based on the dissipative shunting technique with a balancing current of up to 500 mA[27] (Figure 1a). The balancer contains a transistor–resistor pair for each SC that shunts current and discharges the corresponding SC if it reaches the designed voltage limit of 1.25 V.

The CC is composed of components and materials that are compatible with roll-to-roll (R2R) energy materials. The electronic components were selected for their low profile and ability to be integrated with the flexible PV and SCs. At the scale of commercial production, components that are more flexible could be used, resulting in a more flexible CC. The circuit layout occupies a 1453 mm^2 area with a fill factor of 64.2% (power traces only).

Conventional PV power electronics typically use printed circuit boards (PCB) made of rigid fiber glass and optimized thermally. The presented polyimide CC has an overall 0.5 J $\cdot$ K^{-1} specific heat capacity. Although this value is almost six times lower than for fiber-glass PCBs (2.8 J $\cdot$ K^{-1}), the detected worst-case power loss (98.6 mW, Figure 3), leads to a rate of heating that is less than 0.2 K $\cdot$ s^{-1}. At an ambient temperature of 25°C and operating at 98.6 mW, the transistor junction temperature of the boost circuit was measured to stabilize at 51.6°C, where the thermal resistance is calculated from the footprint of the surface-mount active components in the circuit layout. This junction temperature neither affects the operation of the electronic components nor exceeds the limit of 80°C of the passive components or 150°C of the flexible substrate itself.

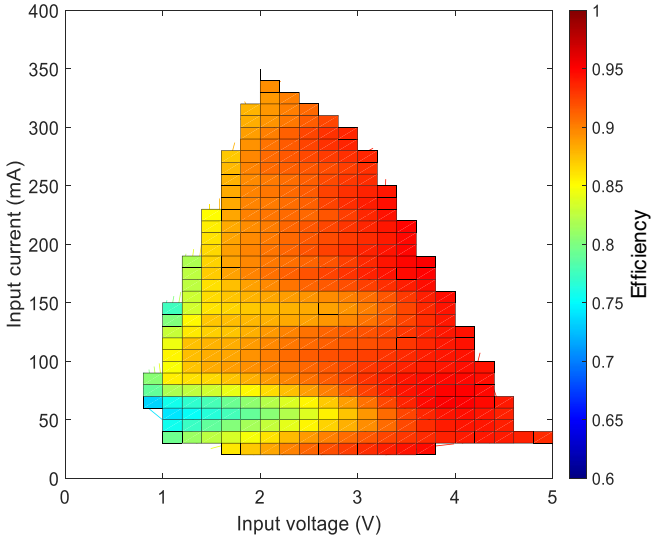

Figure 3. CC operational efficiency as a function of the input voltage and current that is received from the PV.

The power efficiency of the CC was sampled for the entire operation range (see Figure 3) and exceeds 90% for input power from the PV larger than 200 mW, which is compatible with already commercially available flexible PVs that operate at > 2V and > 100mA in standard illumination conditions. As typical for boost converters, the efficiency drops for very low input voltages.

Comparison of charging with and without conversion and control circuit.—As mentioned earlier, a simple serial connection of a PV with SCs is inefficient for energy harvesting and will not fully use the storage capacity of the SCs. To quantify the benefit of the CC, a PV connected directly in series to 4 SCs was compared to the same system with the CC. The systems were compared by charging 4 SCs with equal capacitances (1 F) using illumination intensities of 1 sun and 0.75 suns. These results are discussed in section Comparison of equal capacitance SC charging directly and with a CC. The measurement with 1 sun intensity was repeated in section One sun charging of SCs with non-equal capacitances using 4 SCs of unequal capacitances.

Comparison of equal capacitance SC charging directly and with a CC.—Figure 4 and Figure 5 compare the charging of a bank of 4 SCs of equal capacitance using photocurrent from a PV both directly and with the CC. The maximum power point of the PV was measured to occur at about 1.75 V in both illumination cases. In the system without the CC (Figures 4a, 4c), the PV power is at the maximum power point (MPP) only briefly as the MPP depends on both the illumination intensity and SC bank voltage. For the 1 sun (Figure 4a) and 0.75 sun (Figure 4c) illumination, the power at the MPP (red line and axis) is measured to be 200 mW and 140 mW, respectively. The rising voltage of the charging SC bank (dashed blue line) shifts the operation point of the PV (black line). When the voltage crosses the MPP, the output power of the PV transiently peaks (see Figure 4). Due to the narrow peak and low power levels before and after, the PV is inefficient for much of the charging process. The photocurrent entirely ceases when the SC bank is charged to the PV open-circuit voltage, at around 15 s in both Figures 4a and 4c with an output voltage of 3 V.

For the system with the CC and MPPT (Figures 4b, 4d), the PV power maintains its maximum for a longer time and the SC bank voltage is independent of the open circuit voltage of the PV. During charging, the PV voltage is first perturbed by the CC to find the MPP and then stabilized at the MPP until the SC bank is charged to 5.2 V. This two-step process can be explained in more detail. During the very first phase until the voltage reaches a minimum level, the converter operates the low-side n-channel transistor at fixed duty cycle and

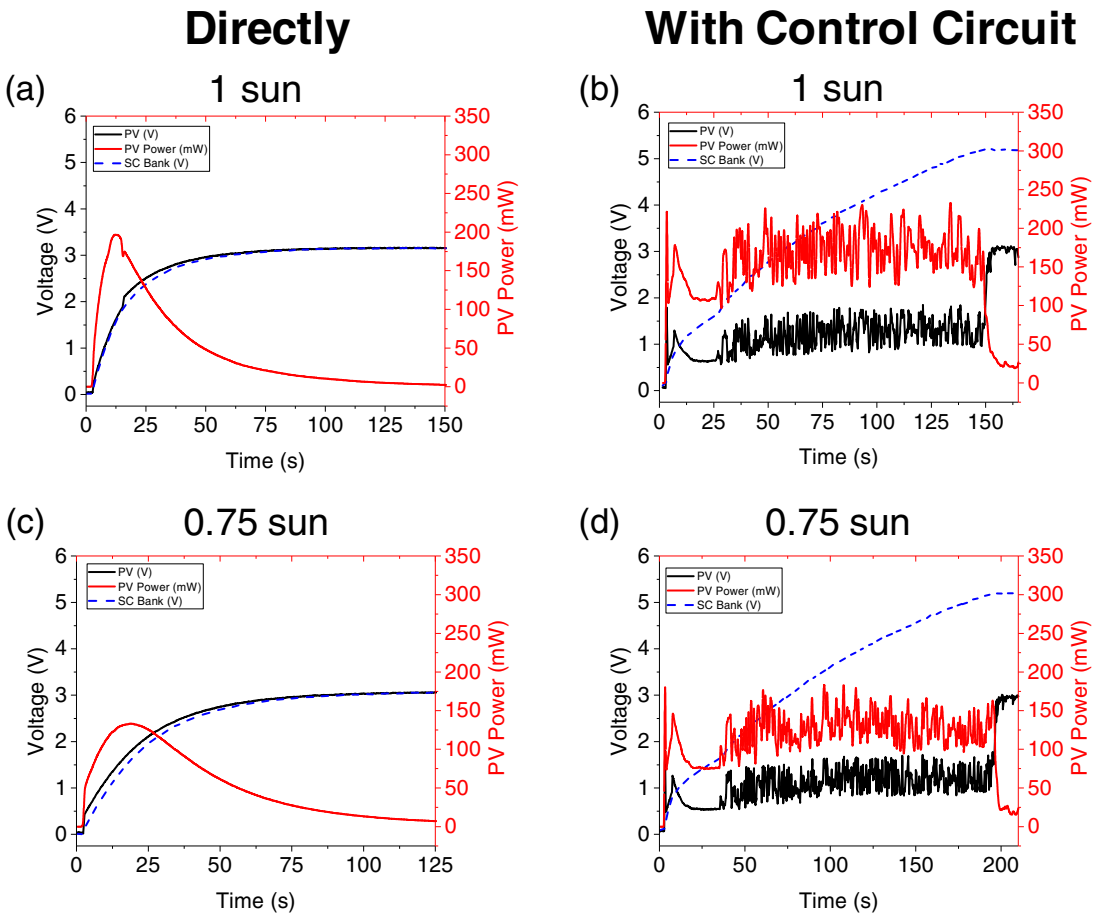

Figure 4. Charging under one sun (a-b) and 0.75 suns (c-d) illumination of 4 SCs without (a,c) and with (b,d) the CC.

therefore constant conversion ratio. Subsequently, the CC perturbs the forward voltage of the PV across a range of 0–1.5 V, and measures the resulting photocurrent, driven by the MPPT function of the CC to find the forward bias voltage of the PV with maximum power output. Furthermore, until the voltage is sufficient to turn the high-side p-channel transistor on reliably at more than 1.5 V, the diode in parallel to the high-side p-channel transistor conducts most of the load current, so that the converter loss dominates and explains initially lower CC efficiency. However, as this output voltage is outside the operation range of the load, this issue only appears during start-up and not during normal steady-state operation. Following this first step, the time-averaged PV voltage occurring at the MPP is then practically fixed due to constant illumination, with only rapid low-amplitude scanning of the MPPT method until the SCs are charged to the maximum boosted voltage of 5.2 V.

Continuous fluctuations of both the PV voltage and power seen in Figures 4b, 4c during this second step is due to continued MPP tracking of the PV voltage. Since the MPP was already found, only minor perturbations are made by the CC. This second step has the benefit of keeping the PV at its MPP during charging in cases of variable sunlight, such as on cloudy days or movement through shaded areas. As seen in the system with the CC (Figures 4b, 4d), the power largely fluctuates around the MPP of the system without the CC (Figures 4a, 4c). This confirms that the MPP algorithm has found the MPP of the PV in the illumination conditions. Moreover, the CC is able to find the MPP of the PV in the initial 25 s, then drive and monitor the PV at its MPP until the SC bank voltage reaches 5.2 V.

As can also be seen for the system with a CC (Figures 4b, 4d), the SC bank voltage is largely independent of the open-circuit voltage of the PV due to the DC-DC boost logic. In both the 1 sun and 0.75 sun illumination cases (Figures 4b, 4d, respectively), an SC bank voltage of 5.2 V can be reached. This is 1.2 V higher than the system without a CC (Figures 4a, 4c). As the energy stored varies as the square of the voltage, this is a large increase in the amount of stored energy. Moreover, the charging of the SC bank is quasi-linear with respect to time and independent of the PV voltage. This is considerably different from the system without the CC, which was both non-linear in charging and largely dependent on the PV voltage.

The boosted voltage and MPPT have a considerable impact on both the rate of energy harvesting from the PV and amount stored in the SC bank. Figure 5 illustrates the energy harvested (a, b) and stored (c, d) with and without a CC at 0.75 sun (a, c) and 1 sun (b, d) illumination intensities.

Energy harvesting.—As can be seen in Figures 5a–5b, the energy harvested in the first 50 s is initially greater for the system without a CC because of the power consumed by the CC and by the time needed for the CC to find the MPP. In the initial 25 seconds when the CC is not entirely functional as the p-channel transistor is not yet activated, the CC is finding the MPP of the PV, and is thus operating the PV at an inefficient voltage-current operating point. This occurs at both illumination intensities in the start-up phase but is not relevant during steady-state operation, when the tracking is on target and where the voltage is above the critical range of the transistor threshold voltage. After 75 s or 50 s of illumination in the 0.75 suns and 1 sun cases, respectively, the PV energy harvested plateaus for the system without the CC (Figures 5a–5b, green and black curves, respectively). The voltage across the SC bank creates a forward bias across the PV, decreasing the photocurrent. In contrast, the system with a CC (Figures 5a–5b, red and blue curves, respectively) continues harvesting solar energy at a roughly linear rate for both illumination

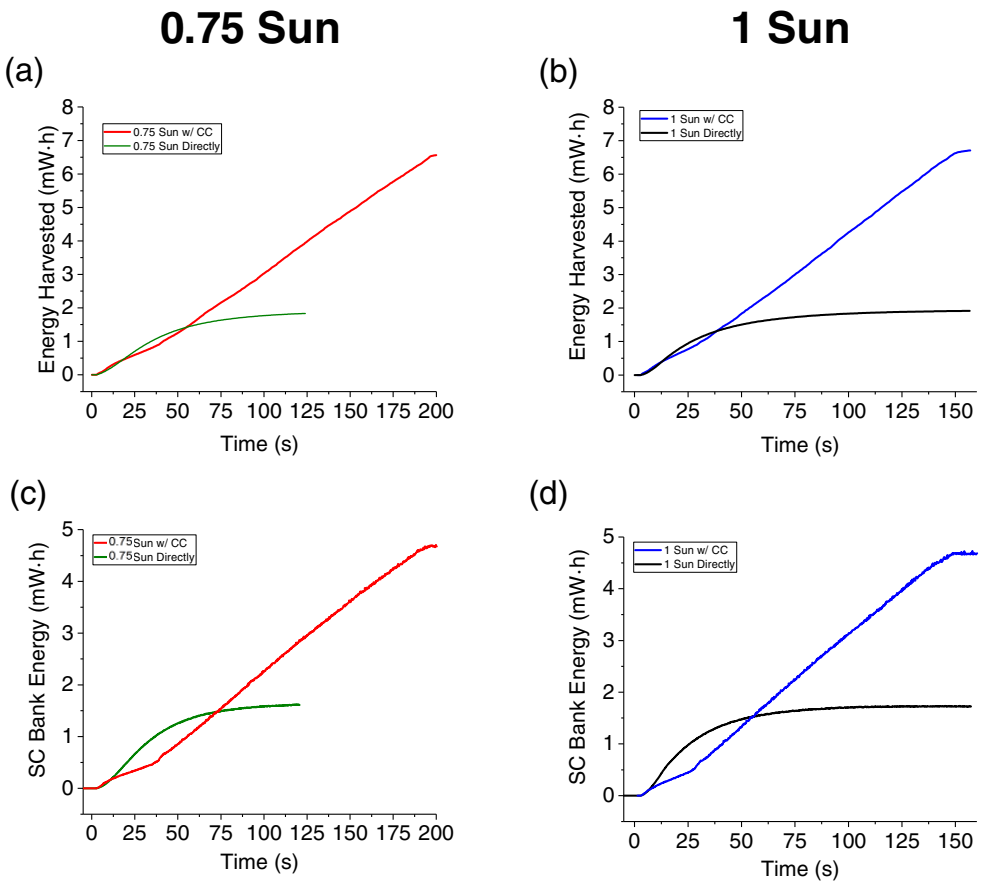

Figure 5. Energy harvested by the PV (a-b) and energy stored in the 4 SCs (c-d) during charging using 0.75 sun (a,c) and 1 sun (b,d) illumination directly or with a CC.

intensities. The energy harvest reaches a maximum only when the boosted voltage of 5.2 V across the SC bank is reached. This occurs at 7 mW · h at both illumination intensities. The energy harvested in the CC system is 3.5x larger than without the CC for two reasons. First, the DC-DC boost circuit allows higher SC-charging voltages, which is controllable, such as 5.2 V instead of ∼3 V without the CC, while the energy content of the capacitors is proportionate to the squared voltage. Second, the CC's balancing circuit can guarantee a set target voltage for each SC, whereas the system without balancing circuit can only charge the SCs in series. In the latter, the smallest SC limits the total stored energy. The open-circuit voltage of the PV limits the SC bank voltage, leading to lower PV energy harvested in the system without the CC.

Energy storage.—The system with the CC is able to store more energy in the SC bank than the system without the CC (Figures 5c–5d) because DC-DC boost logic matches the otherwise incompatible and illumination-dependent voltage levels, enables an increased maximum SC bank voltage, and thus fully utilizes the energy storage capacity in the SC bank. Additionally, the MPPT of the PV accumulates constant photocurrent across time, completely charging the SC-bank with circuit-balancing logic. As noted above, in the initial 70 or 50 s in the 0.75 sun and 1 sun intensity cases, respectively, the system without the CC stores more energy because the CC is determining the MPP voltage. For both illumination conditions, 4.75 mW · h of energy is stored in the SC bank with the CC, compared to 1.5 mW · h without a CC resulting in a 3x improvement in energy storage.

One sun charging of SCs with non-equal capacitances.—SCs vary in their overall capacitances, even with the same nominal capacitance due to manufacturing tolerance, ageing, and environmental conditions. Though the variation in commercially produced SCs is actively moderated by quality control measures, the remaining small differences can greatly limit the overall capacitance and therefore energy of SCs connected in series as well as the lifetime.[45] A CC should account for a spread of the properties of the individual SCs in the bank and balance the voltage across each SC to store the maximum possible energy in the SC bank.

Figure 6 shows the differences in charging a SC bank of 1 F (2x), 5 F, and 10 F capacitors using 1 sun illumination. The dashed lines are the voltages across each SC. The solid black line is the overall bank voltage and the solid red line is the energy stored in the SC bank. The charging behavior of the system without a CC (Figure 6a) and with (Figure 6b) is shown. There are three main differences between the two systems. First, the SC bank voltage in the system without a CC (Figure 6a) rises according to the trend described in the previous section and is limited by the PV open circuit voltage. Charge is balanced across the entire bank and results in a larger voltage across the 1 F SCs than the 5 F and 10 F SCs. Once the SC bank voltage reaches the open circuit voltage of the PV, charging of the SC bank ceases, leaving the voltages across each SC different.

For the system with the CC (Figure 6b), the overall SC bank voltage looks like a segmented line versus time. The voltage across each SC is continuously balanced. This leads to the 1 F SCs reaching the maximum voltage of 1.25 V quickly (< 50 s). Once the 1 F SCs are charged, the photocurrent is shunted to the larger SCs (5 F and 10 F). Next, the 5 F SC is charged followed by the 10 F SC. The rate of change in the voltage follows this trend and is the result of larger SCs increasing in voltage more slowly than the smaller SCs.

Second, the rate of energy storage versus time in the SC banks differs greatly between the case without the CC (Figure 6a, red line) and the case with the CC (Figure 6b, red line). Without the CC, the rate of energy storage decays exponentially and follows the rate of

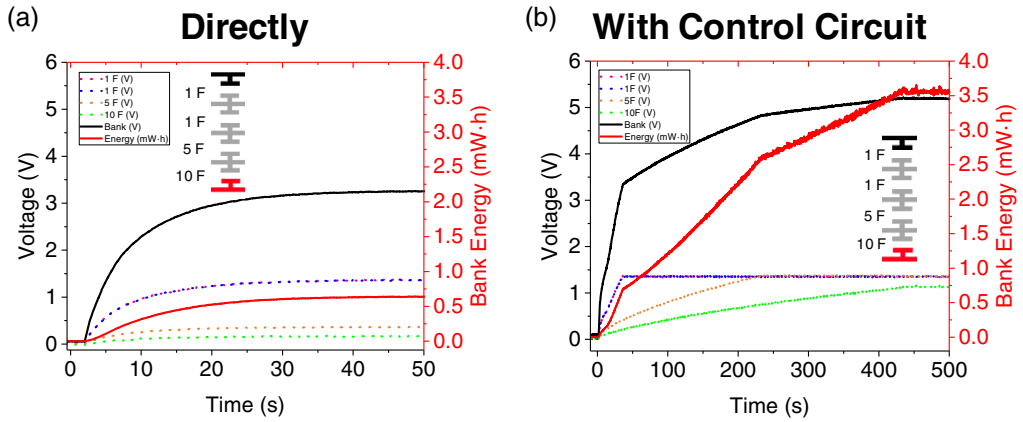

Figure 6. PV charging of non-equal capacitances (a) directly and (b) with the CC where SCs are 1 F (2x), 5 F and 10 F.

change of the SC bank voltage. With the CC, this relationship is decoupled, showing differing rates of voltage increase and energy storage across the SC bank. As each individual SC reaches 1.25 V, the SC bank voltage slope decreases. The slope of the SC bank energy storage curve decreases less, though it is in proportion to the change in slope of the SC bank voltage curve. This is the result of analog dissipative shunting. When a SC reaches its maximum voltage, the current is then shunted down the serially connected SCs to charge the other SCs. The process continues until the SC bank voltage reaches its maximum of 5.2 V. The rate of energy storage in the bank is not changed as greatly because current is redirected from fully charged to incompletely charged SCs. The change in the slope of the energy stored curve across the charging period in the system with a CC are the result of thermal losses from the analog dissipative shunting logic.

Third, the energy stored in the system without the CC is limited by the smallest SC and the number of SCs in series. This is a fundamental drawback to storing charge in serially connected and dissimilar SCs. While the SCs could be carefully matched to have similar capacitance, internal resistance, and leakage, this is a large additional cost that is not compatible wither cost-driven applications such as the one here. Further, even initially well-matched supercapacitors drift apart throughout their lifetime because of different ageing. SCs are commonly connected in series to accommodate a higher operational voltage. The result is a circuit capacitance that is given by

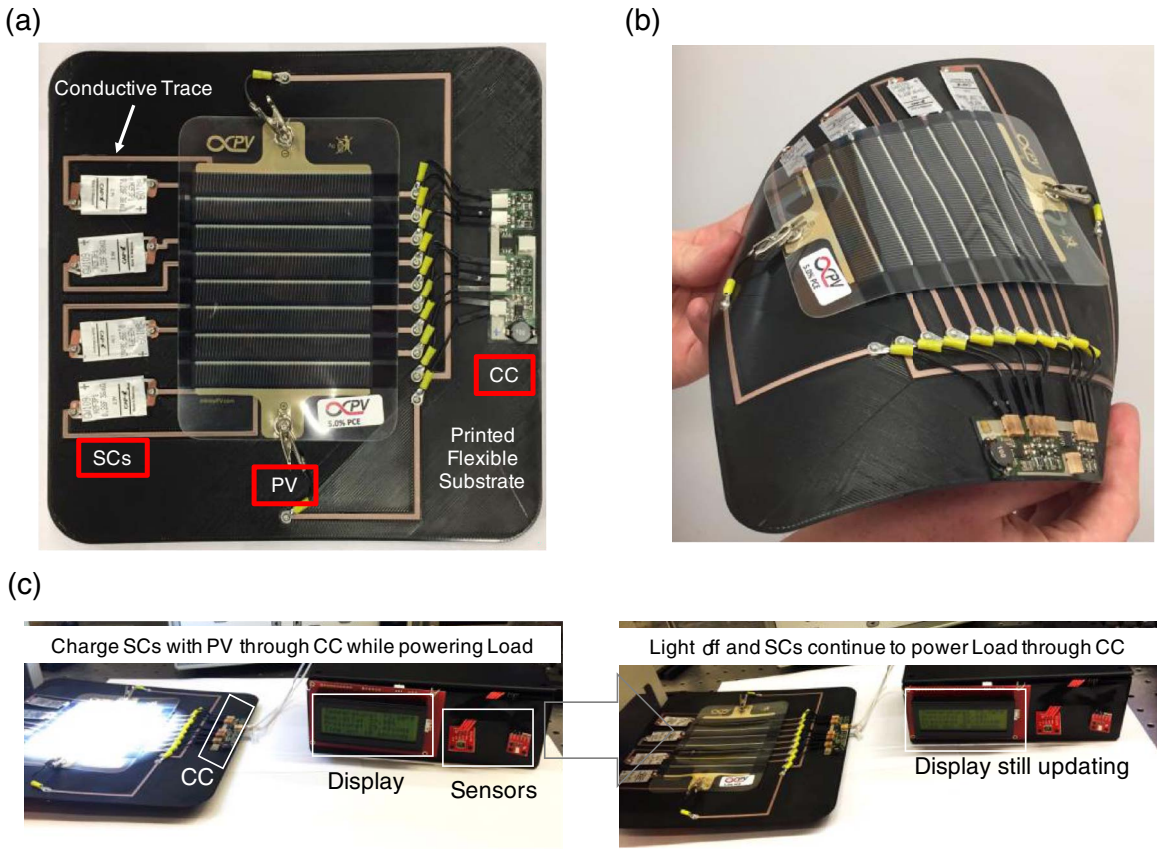

Figure 7. (a) Example flexible substrate using 3D-printed PLA and with Electrifi conductive traces showing potential integration of PV, SCs and CC. (b) Demonstration of the flexibility of the substrate and system components. (c) 1 sun illumination of the OPV charges 4 SCs through the CC while powering a sensor load. (d) Illumination is halted and 20 s later energy stored in the SCs continues to power the load through the CC.

$C_{Tot} = (\sum_1^n \frac{1}{C_i})^{-1}$, where C_{Tot} is the effective circuit capacitance, n is the number of SCs in series, and C_i is the individual capacitance of each SC. The energy stored in the serially connected SCs is then given by, $E_{Tot} = \frac{1}{2} C_{Tot} V^2$, where E_{Tot} is the energy and V is the SC bank voltage. Calculating the energy stored in the SC bank used in Figure 6a without the CC and open-circuit voltage of the PV at an SC bank voltage of 3 V is 0.54 mW · h, the same as the measured value. Adding DC-DC boosted voltage would give a voltage across the SC bank of 5.2 V with an expected energy stored of 1.65 mW · h. However, the CC not only boosts the voltage, but balances it across each SC, charging it to 1.25 V using analogue dissipative shunting logic. As a result, the balancing circuit increases the energy stored in the SC bank to 3.5 mW · h (Figure 6b). This is a greater than 6x increase of energy storage when compared to the system without the CC. Moreover, combined with the DC-DC boost logic, the effective SC bank capacitance with the CC is 0.932 F compared to 0.435 F without the CC. The balancing circuit in the CC reduces the impact of serially connected SCs with dissimilar capacitances.

Practical demonstration of conversion and control circuit with an OPV and flexible SCs.—Wearable technology is of considerable interest presently. Combining wearable technology with a PV, SCs, and a CC in a single textile would provide a method of continuously powering wearable technology without an external power source. Figure 7 shows a practical demonstration of the CC connected through a 3D-printed flexible substrate with conductive traces to a typical wearable sensor load, flexible organic photovoltaic (OPV), and flexible SCs.

The 3D-printed substrate with conductive traces, OPV, and SCs serve as an intermediate step toward the realization of a monolithic and wearable energy fabric. Figure 7a shows the layout of the substrate and components. Figure 7b illustrates the flexibility of the components and the 3D printed substrate. The load comprises a microprocessor; ambient sensors for temperature, pressure, and relative humidity; and a 16 × 2 LCD display. This load is typical for wearable electronics both in technology and power requirements.

Prior to illumination, the load is unpowered and the SCs are discharged. The OPV is then illuminated with 1 sun intensity. Within 1 s, the load boots and displays the first readout of temperature, pressure, relative humidity, and elapsed time on the LCD. The load continues to be powered while excess photocurrent is stored in the SCs. As shown in Figure 7b, the SC bank is charged to its maximum voltage of 5.2 V at 60 s. Once charged, the illumination is turned off and energy stored in the SC bank is then used as a power source for the sensor demonstration. After 20s, the load continues to be powered by the SCs through the CC (Figure 7c). By using larger SCs, the run time could be increased. Replacing the SCs with flexible batteries could increase the run time, however charge–discharge cycling of batteries greatly diminishes their overall capacity. In contrast, the SCs can be cycled 100k or more times, even at high current densities, with little deterioration in their overall capacity and charge-storage efficiency, making SCs a good choice for wearable electronics, where long lifetime is important.

Conclusions

There is an existing need for roll-to-roll (R2R) energy harvesting and storage materials. While individual energy capture and storage components with both high efficiency and R2R compatibility have been demonstrated, integration of these materials in a complete system has not been accomplished. Herein, we presented an important component of an integrated system, a R2R compatible conversion and control circuit (CC) that could greatly improve the integrated performance of R2R energy materials. The CC is capable of max-power-point tracking (MPPT), DC-DC boost of photovoltaic (PV) output, and voltage balancing of four supercapacitors (SCs). The importance of these abilities in utilizing R2R energy material systems is demonstrated through integration with flexible PV, SCs, and a sensor load under two different illumination intensities. It is shown that the same materials can harvest 5x and store 3x more solar energy when using a CC than when not. The CC is demonstrated to improve energy storage in mismatched SC situations by more than 5x through voltage balancing of the serially-connected SCs. A flexible, fully R2R-compatible integrated system was demonstrated by affixing the CC on a flexible 3D-printed circuit board, connecting it with a flexible PV and four flexible SCs, and powering a typical wearable sensor load.

Acknowledgments

The authors acknowledge the National Science Foundation for funding of this research under NSF ECCS-1344745 and NSF ECCS-1608929, as well as the Duke University Energy Initiative for seed funding.

ORCID

J. O. Thostenson https://orcid.org/0000-0002-5494-482X
Z. Li https://orcid.org/0000-0002-4839-2045
C. B. Parker https://orcid.org/0000-0002-7831-1242
A. V. Peterchev https://orcid.org/0000-0002-4385-065X
J. T. Glass https://orcid.org/0000-0002-9554-4398
S. M. Goetz https://orcid.org/0000-0002-1944-0714

References

1. G. Dennler, S. Bereznev, D. Fichou, K. Holl, D. Ilic, R. Koeppe, M. Krebs, A. Labouret, C. Lungenschmied, A. Marchenko, D. Meissner, E. Mellikov, J. Méot, A. Meyer, T. Meyer, H. Neugebauer, A. Öpik, N. S. Sariciftci, S. Taillemite, and T. Wöhrle, "A self-rechargeable and flexible polymer solar battery," *Sol. Energy*, **81**(8), 947 (2007).
2. Y. Galagan, I. G. de Vries, A. P. Langen, R. Andriessen, W. J. H. Verhees, S. C. Veenstra, and J. M. Kroon, "Technology development for roll-to-roll production of organic photovoltaics," *Chem. Eng. Process. Process Intensif.*, **50**(5–6), 454 (2011).
3. S. Logothetidis, "Flexible organic electronic devices: Materials, process and applications," *Mater. Sci. Eng. B*, **152**(1–3), 96 (2008).
4. M.-G. Kang, H. Joon Park, S. Hyun Ahn, and L. Jay Guo, "Transparent Cu nanowire mesh electrode on flexible substrates fabricated by transfer printing and its application in organic solar cells," *Sol. Energy Mater. Sol. Cells*, **94**(6), 1179 (2010).
5. N. Espinosa, R. García-Valverde, A. Urbina, and F. C. Krebs, "A life cycle analysis of polymer solar cell modules prepared using roll-to-roll methods under ambient conditions," *Sol. Energy Mater. Sol. Cells*, **95**(5), 1293 (2011).
6. L. Yang, T. Zhang, H. Zhou, S. C. Price, B. J. Wiley, and W. You, "Solution-Processed Flexible Polymer Solar Cells with Silver Nanowire Electrodes," *ACS Appl. Mater. Interfaces*, **3**(10), 4075 (2011).
7. F. C. Krebs, T. Tromholt, and M. Jørgensen, "Upscaling of polymer solar cell fabrication using full roll-to-roll processing," *Nanoscale*, **2**(6), 873 (2010).
8. J.-S. Yu, I. Kim, J.-S. Kim, J. Jo, T. T. Larsen-Olsen, R. R. Søndergaard, M. Hösel, D. Angmo, M. Jørgensen, and F. C. Krebs, "Silver front electrode grids for ITO-free all printed polymer solar cells with embedded and raised topographies, prepared by thermal imprint, flexographic and inkjet roll-to-roll processes," *Nanoscale*, **4**(19), 6032 (2012).
9. R. Po, A. Bernardi, A. Calabrese, C. Carbonera, G. Corso, and A. Pellegrino, "From lab to fab: how must the polymer solar cell materials design change?–an industrial perspective," *Energy Environ. Sci.*, **7**(3), 925 (2014).
10. I. E. Stewart, A. R. Rathmell, L. Yan, S. Ye, P. F. Flowers, W. You, and B. J. Wiley, "Solution-processed copper–nickel nanowire anodes for organic solar cells," *Nanoscale*, **6**(11), 5980 (2014).
11. S. L. Candelaria, Y. Y. Shao, W. Zhou, X. L. Li, J. Xiao, J. G. Zhang, Y. Wang, J. Liu, J. H. Li, and G. Z. Cao, "Nanostructured carbon for energy storage and conversion," *Nano Energy*, **1**(2), 195 (2012).
12. S. Bae, H. Kim, Y. Lee, X. Xu, J.-S. Park, Y. Zheng, J. Balakrishnan, T. Lei, H. Ri Kim, Y. Il Song, Y.-J. Kim, K. S. Kim, B. Ozyilmaz, J.-H. Ahn, B. H. Hong, and S. Iijima, "Roll-to-roll production of 30-inch graphene films for transparent electrodes," *Nat Nano*, **5**(8), 574 (2010).
13. M. R. Arcila-Velez, J. Zhu, A. Childress, M. Karakaya, R. Podila, A. M. Rao, and M. E. Roberts, "Roll-to-roll synthesis of vertically aligned carbon nanotube electrodes for electrical double layer capacitors," *Nano Energy*, **8**, 9 (2014).
14. K.-H. Choi, J. Yoo, C. K. Lee, and S.-Y. Lee, *Energ Environ Sci.*, **9**, 2812 (2016).
15. J. Yeo, G. Kim, S. Hong, M. S. Kim, D. Kim, J. Lee, H. B. Lee, J. Kwon, Y. D. Suh, H. W. Kang, H. J. Sung, J.-H. Choi, W.-H. Hong, J. M. Ko, S.-H. Lee, S.-H. Choa, and S. H. Ko, "Flexible supercapacitor fabrication by room temperature rapid laser processing of roll-to-roll printed metal nanoparticle ink for wearable electronics application," *J. Power Sources*, **246**, 562 (2014).
16. I. Chung, B. Lee, J. He, R. P. H. Chang, and M. G. Kanatzidis, "All-solid-state dye-sensitized solar cells with high efficiency," *Nature*, **485**(7399), 486 (2012).

17. C.-T. Chien, P. Hiralal, D.-Y. Wang, I.-S. Huang, C.-W. C.-C. Chen, C.-W. C.-C. Chen, and G. A. J. Amaratunga, "Graphene-Based Integrated Photovoltaic Energy Harvesting/Storage Device," *Small*, **11**(24), 2929 (2015).
18. Z. Gao, C. Bumgardner, N. Song, Y. Zhang, J. Li, and X. Li, "Cotton-textile-enabled flexible self-sustaining power packs via roll-to-roll fabrication," *Nat. Commun.*, **7** 11586 (2016).
19. T. Chen, L. Qiu, Z. Yang, Z. Cai, J. Ren, H. Li, H. Lin, X. Sun, and H. Peng, "An Integrated 'Energy Wire' for both Photoelectric Conversion and Energy Storage," *Angew. Chemie Int. Ed.*, **51**(48), 11977 (2012).
20. P. Du, X. Hu, C. Yi, H. C. Liu, P. Liu, H. Zhang, and X. Gong, "Self-Powered Electronics by Integration of Flexible Solid-State Graphene-Based Supercapacitors with High Performance Perovskite Hybrid Solar Cells," *Adv. Funct. Mater.*, **25**(16), 2420 (2015).
21. Y. Fu, H. Wu, S. Ye, X. Cai, X. Yu, S. Hou, H. Kafafy, and D. Zou, "Integrated power fiber for energy conversion and storage," *Energy Environ. Sci.*, **6**(3), 805 (2013).
22. W. Guo, X. Xue, S. Wang, C. Lin, and Z. L. Wang, "An integrated power pack of dye-sensitized solar cell and Li battery based on double-sided TiO_2 nanotube arrays," *Nano Lett.*, **12**(5), 2520 (2012).
23. D. Schmidt, D. Hager Martin, and S. Schubert Ulrich, "Photo-Rechargeable Electric Energy Storage Systems," *Adv. Energy Mater.*, **6**, 1500369 (2015).
24. Q. Brogan, T. O. Connor, and D. S. Ha, in *2014 IEEE International Symposium on Circuits and Systems (ISCAS)*, p. 1412 (2014).
25. W. Jia, X. Wang, S. Imani, A. J. Bandodkar, J. Ramírez, P. P. Mercier, and J. Wang, "Wearable textile biofuel cells for powering electronics," *J. Mater. Chem. A*, **2**(43), 18184 (2014).
26. M. Sippola, E. Oyj, and F. Bescherer, "Reel-to-reel manufacturable, leadless surface mountable, Z-folded planar power transformers," no. Lcc.
27. J. Kundrata and A. Baric, "Design of a planar inductor for DC-DC converter on flexible foil applications," *MIPRO, 2012 Proc. 35th Int. Conv.*, 54 (2012).
28. Y. Xiao, N. P. Jain, J. Barrett, E. J. Rymaszewski, R. J. Gutmann, and T. P. Chow, in Power Semiconductor Devices and ICs, 2001. ISPSD'01. *Proceedings of the 13th International Symposium on*, p. 55 (2001).
29. Y. Xiao, R. Natarajan, T. P. Chow, E. J. Rymaszewski, and R. J. Gutmann, "Flip-Chip Flex-Circuit Packaging for 42V / 16A Integrated Power Electronics Module Applications," **0**(c), 21 (2002).
30. A. B. Lostetter, F. Barlow, A. Elshabini, K. Olejniczak, and S. Ang, "Polymer Thick Film (PTF) and flex technologies for low cost power electronics packaging," *IWIPP 2000 - Int. Work. Integr. Power Packag.*, 33 (2000).
31. J. Dieffenderfer, H. Goodell, S. Mills, M. McKnight, S. Yao, F. Lin, E. Beppler, B. Bent, B. Lee, V. Misra, Y. Zhu, O. Oralkan, J. Strohmaier, J. Muth, D. Peden, and A. Bozkurt, *IEEE Journal of Biomedical and Health Informatics*, **20**, 1251 (2016).
32. F. Axisa, P. M. Schmitt, C. Gehin, G. Delhomme, E. McAdams, and A. Dittmar, "Flexible Technologies and Smart Clothing for Citizen Medicine, Home Healthcare, and Disease Prevention," *IEEE Trans. Inf. Technol. Biomed.*, **9**(3), 325 (2005).
33. M. Chen, S. Gonzalez, A. Vasilakos, H. Cao, and V. C. M. Leung, "Body Area Networks: A Survey," *Mob. Networks Appl.*, **16**(2), 171 (2011).
34. M. Ermes, J. Parkka, J. Mantyjarvi, and I. Korhonen, "Detection of Daily Activities and Sports With Wearable Sensors in Controlled and Uncontrolled Conditions," *IEEE Trans. Inf. Technol. Biomed.*, **12**(1), 20 (2008).
35. A. Pantelopoulos and N. G. Bourbakis, "A Survey on Wearable Sensor-Based Systems for Health Monitoring and Prognosis," *IEEE Trans. Syst. Man, Cybern. Part C (Applications Rev.*, **40**(1), 1 (2010).
36. R. Paradiso, G. Loriga, and N. Taccini, "A Wearable Health Care System Based on Knitted Integrated Sensors," *IEEE Trans. Inf. Technol. Biomed.*, **9**(3), 337 (2005).
37. S. Patel, H. Park, P. Bonato, L. Chan, and M. Rodgers, "A review of wearable sensors and systems with application in rehabilitation," *J. Neuroeng. Rehabil.*, **9**(1), 21 (2012).
38. B. S. Shim, W. Chen, C. Doty, C. Xu, and N. A. Kotov, "Smart Electronic Yarns and Wearable Fabrics for Human Biomonitoring made by Carbon Nanotube Coating with Polyelectrolytes," *Nano Lett.*, **8**(12), 4151 (2008).
39. C.-C. Yang and Y.-L. Hsu, "A Review of Accelerometry-Based Wearable Motion Detectors for Physical Activity Monitoring," *Sensors*, **10**(8), 7772 (2010).
40. W. Zeng, L. Shu, Q. Li, S. Chen, F. Wang, and X.-M. Tao, "Fiber-Based Wearable Electronics: A Review of Materials, Fabrication, Devices, and Applications," *Adv. Mater.*, **26**(31), 5310 (2014).
41. Y. Hao and R. Foster, "Wireless body sensor networks for health-monitoring applications," *Physiol. Meas.*, **29**(11), R27 (2008).
42. S. J. Preece, J. Y. Goulermas, L. P. J. Kenney, D. Howard, K. Meijer, and R. Crompton, "Activity identification using body-mounted sensors–a review of classification techniques," *Physiol. Meas.*, **30**(4), R1 (2009).
43. G. K. Ottman, H. F. Hoffman, and G. A. Lesieutre, *IEEE Transactions on Power Electronics*, **18**, 696 (2003).
44. P. F. Flowers, C. Reyes, S. Ye, M. J. Kim, and B. J. Wiley, "3D printing electronic components and circuits with conductive thermoplastic filament," *Addit. Manuf.*, **18**, 156 (2017).
45. D. Linzen, S. Buller, E. Karden, and R. W. De Doncker, "Analysis and evaluation of charge-balancing circuits on performance, reliability, and lifetime of supercapacitor systems," *IEEE Trans. Ind. Appl.*, **41**(5), 1135 (2005).